Desalination and Water Treatment
www.deswater.com

doi: 10.5004/dwt.2019.24229

158 (2019) 330–342
August

Adsorption of Methylene Blue onto nano SBA-15 mesoporous material from aqueous media: kinetics, isotherms and thermodynamic studies

Qing-Zhou Zhai*, Yuan Dong, Heng Liu, Qing-Shuang Wang

Research Center for Nanotechnology, South Campus, Changchun University of Science and Technology, 7186 Weixing Road, China, Tel. +86 431 85583118; Fax: +86 431 85383815; email: zhaiqingzhou@163.com (Q.-Z. Zhai)

Received 30 December 2018; Accepted 7 April 2019

ABSTRACT

Santa Barbara Amorphous (SBA-15) molecular sieve was prepared by hydrothermal synthesis method. The surface and pore structure of SBA-15 were characterized by low-temperature N_2 adsorption isotherm, X-ray diffraction (XRD), transmission electron microscopy (TEM), scanning electron microscopy (SEM) and Fourier transform infrared (FT-IR) spectroscopy. Methylene blue dye solution was adsorbed by the synthetic SBA-15, the best adsorption condition and the maximum adsorption capacity of methylene blue by SBA-15 were obtained by experiments, and the maximum adsorption capacity is 223 mg g^{-1}. The kinetics of the adsorption of methylene blue by SBA-15 was in accordance with the quasi-second-order kinetic equation. The results were analyzed by Langmuir and Freundlich adsorption isotherm model, and the adsorption of methylene blue on SBA-15 was in accord with the Freundlich adsorption isotherm model. The Gibbs free energy changes during the adsorption $\Delta G° < 0$ can judge that the adsorption process is spontaneous. The enthalpy change in the adsorption process is –16.623 kJ mol^{-1}, that is $\Delta H° < 0$, indicating that the adsorption process is an exothermic reaction. The negative value of entropy indicates that the adsorption process is a process of entropy reduction. The composite materials after adsorption were characterized by powder XRD, SEM, FT-IR spectra, low temperature N_2 adsorption-desorption. The characterization results show that the composite materials still retained the skeleton structure of the mesoporous materials, but the order degree of the composites was decreased. After adsorption, the average pore size, total pore volume and specific surface area of the composite materials are lower than those of the mesoporous materials before adsorption, indicating that the pores of mesoporous materials were partly filled and blocked. This indicated that the dye molecules were contained in the mesoporous channels.

Keywords: Methylene blue; Adsorption; SBA-15

1. Introduction

Dyes play an important role in our daily lives [1]. It has a wide range of applications in technology and industry, including the traditional use, such as textile printing and dyeing, and other daily-use articles. With the development of science and technology, the dyes have a number of new uses, such as laser dyes, these dyes are used for organic light-emitting diodes [2], liquid crystal display [3], optical data storage and fluorescent labeling, etc. [4]. The wide application of dyes brings not only convenience to our life but also problems that cannot be ignored. Dye-contaminated wastewater contains dyes and the residual colored compounds of a variety of chemical additive. The colored wastewater that flows into the river reduces the penetration of light, reduces the phenomenon of photosynthesis, causing harm to fish and some aquatic organisms. Methylene blue is widely used in our daily life. Although methylene blue has no very strong danger, it also causes some harmful effects, including paper dyeing, temporary

* Corresponding author.

hair coloring, cotton dyeing, wool and paper material coating. It can cause some harmful effects, such as accelerating heart rate, vomiting, shock, jaundice, limb paralysis and human tissue necrosis [5,6].

There are some methods for the removal of dyes in aqueous solution, such as photocatalytic degradation method [7,8], sonochemical degradation method [9], micelle enhanced ultrafiltration method [10], cationic exchange membrane method [11], electrochemical degradation method [12], adsorption/precipitation method [13], etc. And it is well known that chemical degradation method and ion exchange method produce some harmful substances, give water body the possibility to bring the second pollution. In terms of initial cost, flexibility, simplicity of design and ease of operation, the adsorption method is superior to other techniques that have been found in the reuse of water. Also, adsorption cannot lead to the formation of harmful substances to avoid the second pollution [14]. The most common commercial adsorbent is activated carbon, and activated carbon as a result of its high cost makes the adsorption method become a luxury one. In recent years, some scientists have also excavated some new adsorbents, such as garlic skin [5], swede rape straw modified by tartaric acid [15], jute fiber carbon [16,17]. For agricultural waste material as adsorbent, the combination force between dye and adsorbent is weak and adsorption capacity is small. In recent years, Javadian et al. [18] and Sharma et al. [19] proposed polyaniline/γ-alumina nancomposite, starch/poly (alginic acid-cl-acrylamide) nanohydrogel, etc. as adsorbents to adsorb dyes. The adsorption efficiency has been improved.

Mesoporous silica material has larger surface area and pore channel volume, which provide a good carrier for drug immobilization, catalytic reaction, adsorption and separation reaction. Chaudhuri et al. [20,21] studied some mesoporous silica materials for removal of some dyes and achieved good adsorption effects. For removal of methylene blue from aqueous medium, steam activated carbon from lantana camara stem [22], hydrophobic activated carbons/propylene diamine basic activated carbons [23], activated lignin–chitosan composite [24], activated carbon prepared from dross licorice by ultrasonic method [25], magnetite@silica@pectin hybrid nanocomposites [26] Fe_3O_4@APS@AA-co-CA MNPs [27], recyclable magnetite-loaded palm shell-waste based activated carbon [28], NH_2-MIL-101 (Al) [29], MIL-53 (Al)-NH_2 [30], Fe_3O_4@AMCA-MIL53 (Al) [31] have been evaluated as adsorbents. In a series of mesoporous molecular sieves, one of the most typical representatives is Santa Barbara Amorphous (SBA-15) [32]. SBA-15 and MCM-41 synthesized for the first time, both are 2-dimensional hexagonal mesostructure. Comparing them, SBA-15 has more advantages, because it overcomes the shortcomings of the poor hydrothermal stability of MCM-41. SBA-15 has larger pore diameter and wall thickness, as well as the larger pore size and specific surface area of SBA-15 mesoporous molecular sieve, which makes it become a better new type adsorbent.

In this study, SBA-15 molecular sieve was synthesized by hydrothermal method, and was used to adsorb methylene blue dye from solution. The influence of the experimental conditions on the adsorption capacity of methylene blue was studied by the experimental conditions of solution pH, contact time, initial dye concentration, the amount of adsorbent and so on. The kinetics and thermodynamics of this adsorption were studied. The SBA-15 and (SBA-15)-methylene blue after adsorption were characterized, the results of the characterization were analyzed, so that the adsorption principle is clearer.

2. Materials and methods

2.1. Materials

Table 1 gives the information on methylene blue. Methylene blue (MB, Tianjin Guangfu Research Institute of Fine Chemical Industry, China), tri-block copolymer (polyethylene glycol-block-propylene glycol-block-polyethylene glycol, Sigma-Aldrich), tetraethyl orthosilicate (TEOS, Shanghai First Factory of Reagent, China), hydrochloric acid (Beijing Chemical Plant, China), phosphoric acid (Kemi'ou Chemical Reagent Development Center of Tianjin City, China), acetic acid (Beijing Chemical Plant, China), boric acid (Beijing Chemical Plant, China) and sodium hydroxide (Beijing Chemical Plant, China) were used in this work. All the chemical reagents used in the experiments were analytically pure, and all the water used were deionized water.

2.2. Synthesis and characterization of material

2.2.1. Synthesis of material

2.0 g of tri-block copolymer poly(ethylene glycol)-block-poly(propylene glycol)-block-poly(ethylene glycol) was dissolved in 15.0 g of water and 60.0 g of 2 mol L^{-1} hydrochloric acid solution, stirred up to complete dissolution. At 40°C, 4.25 g of TEOS was added, stirred for 24 h and then transferred into an autoclave. At 100°C, crystallization was made for 48 h at the constant temperature. After the crystallization was finished, filtration was made and the product was washed using deionized water. The product was dried at room temperature. The above product was placed in a ceramic crucible, put into a muffle oven and calcined at 550°C for 24 h to eliminate the tri-block copolymer

Table 1
Basic information of methylene blue

Common name	Methylene blue (Beautiful blue)
Chemical formula	$C_{16}H_{18}ClN_3S \cdot 3H_2O$
Relative molecular mass (g mol^{-1})	373.90
Molecular volume (cm^3 mol^{-1})	241.9
Molecular diameter (nm)	0.80
λ_{max} (nm)	664
No. CAS	7220-79-3
Structural formula	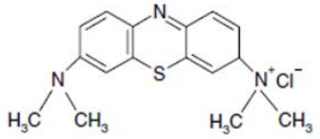

template. A SBA-15 mesoporous material white powder was obtained [33,34].

2.2.2. Characterization of material

Crystal structure and periodic characteristics of information were determined using D5005 X-ray diffractometer (Siemens Company, Germany) determination, Cu–K_α target, λ = 1.540560 Å. Operating voltage is 50 kV, the operating current is 150 mA. Scanning range is 0° ~ 10°, the step size is 0.02 (°) step^{-1}. The particle morphology and size of the samples were observed on the scanning electron microscope and the scanning electron microscopic photograph was measured by field emission scanning electron microscope (XL30 Philips, Netherland). High-resolution transmission electron microscopic photograph was obtained to observe the structure morphology of the sample under the condition of 200 kV as the working voltage on a Tecnai G2 F20 FEI field emission transmission electron microscope. Low-temperature nitrogen adsorption–desorption was measured under liquid nitrogen 77 K conditions on ASAP 2020 V3.01 H type adsorption analyzer (Micromeritics, U.S.A). Data were calculated by Bdb (Broekhoff and de Boer) method [35], the specific surface area was determined according to BET (Brunauer–Emmett–Teller) method [36], the pore size distribution was analyzed by BJH (Barrett-Joyner-Halenda) method [37], low temperature nitrogen adsorption–desorption was used to observe the pore volume, pore size and specific surface area of mesoporous materials. Fourier transform infrared (FT-IR) spectra were recorded on a Nicolet 5DX-FTIR instrumentation made in the American Mike Company. Powder sample in experiments was tableted using KBr (sample proportion, 1% in weight, and the proportion of KBr, 99% in weight). The operation conditions were a resolution of 4 cm^{-1}, scan 32 times, scan wavenumber range 400–4,000 cm^{-1}. The absorbance of methylene blue was determined by a 722S type ultraviolet visible spectrophotometer.

2.3. Study of the adsorption of methylene blue by SBA-15

2.3.1. Effect of solution pH value on the adsorption amount of methylene blue

Weigh 0.005 g of SBA-15 and place it in a 100 mL beaker, add 20 mL of methylene blue solution with a concentration of 6 mg L^{-1}. The pH value was adjusted to 3, 4, 5, 6, 7, 8, 9, 10, 11, 12 and 13, respectively. Stir it at room temperature 25°C ± 1°C for 40 min with a stirring speed of 200 rpm, and centrifuge for 15 min at 6,000 rpm. The supernatant was taken measuring the absorbance, study the different effect of solution pH on the adsorption amount of methylene blue. The adsorption amount of methylene blue at adsorption equilibrium and the amount of adsorption at time t were determined by the following formula:

$$q_e = \frac{\left(C_0 - C_e\right)}{m} \times V \tag{1}$$

Here C_0 and C_e (mg L^{-1}) are liquid concentration at the initial and equilibrium, q_e (mg g^{-1}) is the equilibrium adsorption amount, V (L) is the volume of solution, m (g) is the mass of adsorbent.

$$q_t = \frac{\left(C_0 - C_t\right)}{m} \times V \tag{2}$$

Here C_0 and C_t (mg L^{-1}) are liquid concentration at the initial time and at the time of t (min), respectively, q_t (mg g^{-1}) is the adsorption amount at time t (min), V (L) is the volume of the solution, m (g) is the amount of adsorbent.

2.3.2. Effect of adsorbent dosage on adsorption amount of methylene blue

Weigh 0.002, 0.005, 0.01, 0.015 and 0.02 g of SBA-15 and put in 100 mL beaker, respectively, and add 20 mL of the methylene blue solution at 6, 15 and 30 mg L^{-1} and adjust pH = 9, stirring at room temperature 25°C ± 1°C for 40 min with a stirring speed of 200 rpm. The supernatant was taken after centrifugation at 6,000 rpm for 15 min to measure the absorbance, and the influence of different adsorbent dosage on the adsorption amount of methylene blue.

2.3.3. Effect of contact time on the adsorption amount of methylene blue

Take 0.005 g of SBA-15 and place it into a 100 mL beaker, put in 20 mL of methylene blue solution of concentration 6 mg L^{-1}, adjusting pH = 9 at room temperature 25°C ± 1°C, stirring for 2, 5, 8, 10, 15, 20, 30 and 40 min with a stirring speed of 200 rpm. After centrifugation for 15 min at 6,000 rpm, the supernatant was taken and the absorbance was measured and the effect of different contact time on the adsorption amount of methylene blue was studied.

2.3.4. Adsorption kinetics

Weigh 0.005 g of SBA-15 and place it in a 100 mL beaker, add 20 mL of concentration of 3, 6, 9, 12 and 15 mg L^{-1} solution with (pH = 9.0). At room temperature 25°C ± 1°C, the solution was stirred for 2, 5, 8, 10, 15, 20, 25, 30 and 40 min with a stirring speed of 200 rpm to centrifuge for separation, and the supernatant was taken to measure the absorbance and the concentration of methylene blue was calculated, The adsorption capacity was calculated by Eqs. (1) and (2). In order to study the adsorption reaction mechanism, the simplified dynamic model of the adsorption reaction was used to make analysis, including the quasi-first-order kinetic model and the quasi-second-order kinetic model.

Quasi-first-order kinetic model [38–40] is:

$$\ln\left(q_e - q_t\right) = \ln q_e - \frac{k_1}{2.303} \times t \tag{3}$$

Here k_1 (min^{-1}) is a quasi-first-order kinetic rate constant, q_e (mg g^{-1}) and q_t (mg g^{-1}) are the amount of dye adsorbed at equilibrium and at time t (min), respectively.

Quasi-second-order kinetic model [39–41] is:

$$\frac{t}{q_t} = \frac{1}{k_2 q_e^2} + \frac{t}{q_e} \tag{4}$$

Here k_2 (g mg^{-1} min^{-1}) is the rate constant of quasi-second-order kinetic adsorption principle, q_e (mg g^{-1}) and q_t (mg g^{-1}) are the amount of dye adsorbed at equilibrium and at time t (min), respectively.

2.3.5. Adsorption isotherm

Weigh 0.005 g of SBA-15 and put it in a 100 mL beaker, add 20 mL of methylene blue concentration 3, 6, 9, 12 and 15 mg L^{-1} (pH = 9.0). At 277.15, 298.15 and 308.15 K, after the solution was stirred with a stirring speed of 200 rpm for equilibrium state, centrifuged for separation, and the supernatant was taken to measure the absorbance and the concentration of methylene blue was calculated. The equilibrium adsorption amount was calculated by Eq. (2) and the adsorption isotherm was drawn. The adsorption equilibrium isotherms include the Langmuir adsorption isotherm and the Freundlich adsorption isotherm.

The Langmuir isotherm is described by the following equation [39,40,42–44]:

$$\frac{C_e}{q_e} = \frac{1}{Q_0 b} + \left(\frac{1}{Q_0}\right) \times C_e \tag{5}$$

Here C_e (mg L^{-1}) is equilibrium constant, q_e (mg g^{-1}) is the amount of the adsorbate adsorbed by adsorbent, Q_0 is theoretical saturation adsorption capacity (mg g^{-1}), b is Langmuir (mL mg^{-1}) adsorption constant.

The linear form equation of Freundlich is [39,40,45] as follows:

$$\ln q_e = \ln K_F + \frac{1}{n} \ln C_e \tag{6}$$

where q_e (mg g^{-1}) is the amount of adsorption at equilibrium, C_e (mg L^{-1}) is the concentration of MB at equilibrium. K_F and n is Freundlich constant. K_F is Freundlich adsorption isotherm constant, indicating adsorption degree. And 1/n represents the adsorption strength. 1/n is usually less than 1 because the first use has the mesh with the highest binding energy and then the mesh of use is weaker mesh in turn.

3. Results and discussion

3.1. Characterization of SBA-15

According to the synthesis method [33,34], the yield of the as-synthesized material was 95.5%. Fig. S1 is the X-ray diffraction (XRD) for mesoporous materials SBA-15. From the figure, it can be observed that the mesoporous material prepared has obvious characteristic diffraction peaks at the 2θ = 0.94°, 1.62°, 1.84°, 2.44°. The correspond to the interplanar diffraction of (100), (110), (200), (210), respectively, showing that the material has an ordered mesoporous structure. The structural properties of SBA-15 are shown as Table S1.

SBA-15 low-temperature nitrogen adsorption isotherm and pore size distribution are shown in Figs. S2 and S3, respectively. From Fig. S2, it can be seen that the isotherm of SBA-15 is type IV in the IUPAC classification (Bruno's definition) and shows a H1- hysteresis loop, showing that the channels are cylindrical pore shape. In the characteristic hysteresis loop of low-temperature nitrogen adsorption–desorption isotherm there is one obvious adsorption and desorption branch. The steep adsorption and desorption branches can show that the prepared mesoporous SBA-15 has a narrow pore size distribution. In the adsorption–desorption isotherm, the molecules first are adsorbed on the surface of the molecular sieve in the form of a single molecule, and the multiple molecular layer adsorption does not occur until the pressure is high enough. In the relative partial pressure range (p/p_0) of 0–0.658, with the increase of the relative pressure the molecules adsorbed on the outer surface of the mesoporous surface in the form of single layer to multiple layer, and the volume of nitrogen adsorbed increased. Since the beginning of capillary condensation is in progress at cyclic annular adsorption film surface on the hole wall, and the desorption starts from spherical meniscus, thus in the adsorption–desorption isotherm exists a hysteresis loop.

Fig. S4a is the analysis figure of SBA-15 by scanning electron microscopy (SEM). From the figure SBA-15 wheat-like structure can be seen, the average particle diameter of SBA-15 is 333 ± 10 nm. Fig. S4b is the analysis of SBA-15 by transmission electron microscopy, it can be seen from the figure that the mesopore channels of SBA-15 are parallel to each other. The intersecting surface presented hexagonal arrangement and orderly "honeycomb" porous structure.

Infrared spectrum is mainly used for vibration characterization of framework materials, for the analysis of material structure and chemical bond contained, and also for the analysis of the interaction between substances. It is widely used in the characterization and identification of various chemical substances. Fig. S5 is the infrared spectrum of the SBA-15 from wavenumber 4,000 cm^{-1} to wavenumber 400 cm^{-1}. 466 cm^{-1} is assigned to T–O bend; 801 cm^{-1} is assigned to the symmetric stretching vibration; 1,092 cm^{-1} is assigned to the asymmetric stretching vibration; 3,434 cm^{-1} is water or vibration absorption peak of surface hydroxyl groups.

3.2. Effect of solution pH, adsorbent dosage and adsorption time on the adsorption of methylene blue

In the process of the dye adsorption, the pH value of the solution plays an important role in the adsorption amount of the dye [46,47]. It can be seen from Fig. S6 that the adsorption capacity over pH 3–8 increased with the increase in pH. When pH was higher than 9 (9–13), the adsorption capacity of methylene blue decreased with the increase of pH and the adsorption amount of methylene blue was maximum at pH 8–9. Under the acidic condition, the positive charge carried on the SBA-15 surface increases. And the methylene blue is a cationic dye, so the adsorption capacity of methylene blue is low at this time. And there is a lot of Na^+ in alkaline solution, a large number of Na^+ and methylene blue competes for the adsorption sites on the SBA-15 surface, thereby reducing the amount of adsorption of methylene blue [48].

Influence of adsorbent amount on dye adsorption amount can be seen from Fig. S7. The figure displays the results that for three different initial concentrations of methylene blue solution with the increase of the amount of adsorbent, the adsorption capacity of methylene blue decreased. This is because SBA-15 provides a large number

of adsorption sites. With the increase of adsorbent dosage, the adsorption sites are also continuously increased, thus the competition between the cations that the methylene blue dye provides is reduced to make the adsorption amount of methylene blue be decreased. However, when the adsorbent dosage was the same, the higher the initial concentration of dye, the larger the adsorption amount. This indicates that the initial concentration of dye has a promoting effect for the dye adsorption. The dye concentration is high, the opportunity to contact the dye molecule with the adsorption point sites of the mesoporous material is large, leading to adsorption amount to be large.

In accordance with the experimental method of Section 2.3.3 operation was made, the results obtained are as shown in Fig. S8. As can be seen from Fig. S8, the adsorption of dye by the mesoporous materials was completed in a very short period of time and at 10 min the adsorption equilibrium was reached. The maximum adsorption capacity and the maximum adsorption removal efficiency of this adsorption system for methylene blue are 223 mg g^{-1} and 97.5%, respectively. Table 2 gives some comparison of sorption capacity of various adsorbents for methylene blue adsorption [22–31]. It can be seen that this mesoporous material can become a better adsorbent for the adsorption of dyes with high efficiency.

3.3. Adsorption kinetics

The adsorption kinetic experimental results of Section 2.3.4 were fitted by the quasi-first-order kinetic equation and the quasi-second-order kinetic equation (Eqs. (3) and (4)) to obtain the results as Figs. 1a and b show. Fig. 1a is quasi-first-order kinetic equation linear fitting chart, Fig. 1b is quasi-second-order kinetic equation linear fitting chart and the kinetic related parameters obtained are shown in Table 2. R_1^2 and R_2^2 are correlation coefficients of the quasi-first-order

Table 2
Comparison of various adsorbents: adsorption capacity for methylene blue dye from aqueous medium

Adsorbent	Adsorption capacity (mg g^{-1})	Max C_0 (mg L^{-1})	Reference
Steam-activated carbon from *Lantana camara* stem	19.84	200	[22]
Hydrophobic activated carbons (propylene diamine basic activated carbons)	34.70 (182.0)	700	[23]
Activated lignin–chitosan composite	36.25	82	[24]
Activated carbon prepared from dross licorice by ultrasonic method	82.90	200	[25]
Magnetite@silica@pectin hybrid nanocomposites	85.18	100	[26]
Fe_3O_4@APS@AA-co-CA MNPs	142.9	20–50	[27]
Recyclable magnetite-loaded palm shell-waste based activated carbon	163.3	–	[28]
NH_2-MIL-101 (Al)	188	20–40	[29]
MIL-53 (Al)-NH_2	208.3	5	[30]
Fe_3O_4@AMCA-MIL53 (Al)	325.62	25–400	[31]
SBA-15	223	30	This study

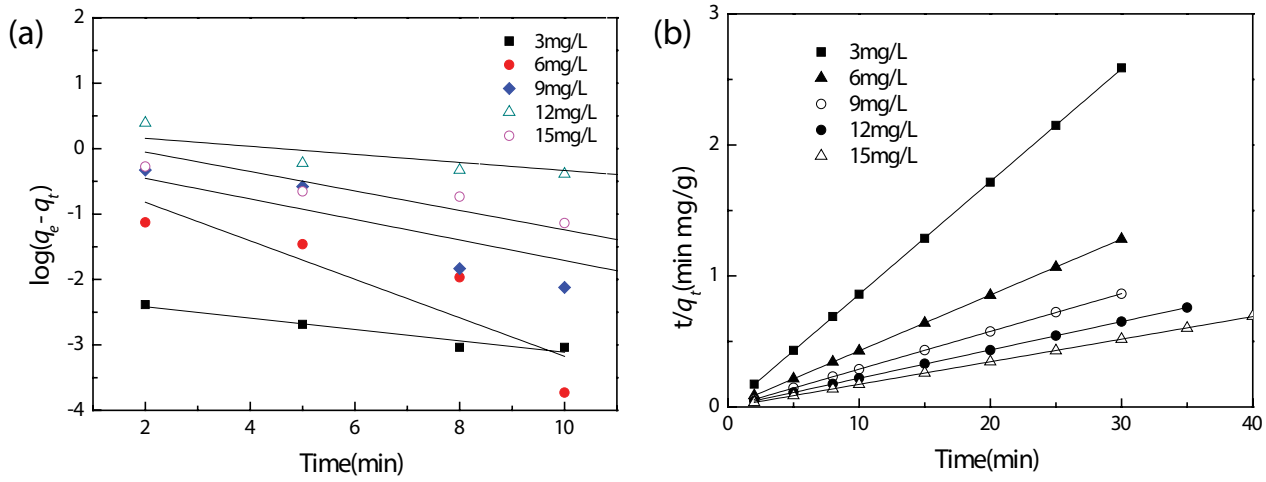

Fig. 1. Adsorption kinetic curve: (a) quasi-first-order kinetic equation linear fitting chart and (b) quasi-second-order kinetic equation linear fitting chart.

Table 3
Kinetic parameters

Concentration (mg L^{-1})	Actual measurement q_e (mg g^{-1})	Quasi-first-order adsorption rate equation			Quasi-second-order adsorption rate equation		
		k_1 (min^{-1})	q_e (mg g^{-1})	R_1^2	k_2 (g mg^{-1} min)	q_e (mg g^{-1})	R_2^2
3	11.616	0.201	0.106	0.91650	–14.286	11.623	0.99998
6	23.408	0.677	0.793	0.68508	0.883	23.452	1.00000
9	34.800	0.361	0.868	0.72232	2.183	34.698	0.99997
12	46.120	0.142	1.324	0.66000	0.157	46.275	0.99996
15	58.080	0.342	1.277	0.84523	0.931	57.971	0.99997

kinetic equation and the quasi-second-order kinetic equation, respectively. From Figs. 1a and b and Table 3 it can be seen that when the kinetic data were fitted by quasi-first-order kinetic equation the deviations are larger, and the calculated deviation of adsorption equilibrium quantity of different concentration and the measured value is larger. When quasi-second-order kinetic equation was used to fit, the correlation coefficient of R_2^2 was greater than 0.9999. Calculation value of the equilibrium adsorption amount of each concentration was basically the same with the actual measured value, so the kinetics of adsorption system more accords with the quasi-second-order kinetic equation.

3.4. Adsorption isotherm

Langmuir adsorption is based on the assumption of monolayer molecular adsorption in a structurally uniform adsorbent, so the adsorption sites are the same and the energy is equal. The adsorbent inside mesh is uniform and a dye molecule occupies a mesh, adsorption action can no longer be carried on this mesh. Freundlich adsorption curve is widely applied to the experiment equation and it is suitable to the experimental data for a very wide range of concentration. This is based on the assumption that the mesh distribution of surface action is different distribution and exponential distribution. Also, it is assumed that there are numerous unreacted meshes, which are available. Figs. 2 and 3 show Langmuir and Freundlich adsorption isotherms, respectively. Based on the square of linear regression correlation coefficient the best fitting model is determined. It can be seen from Table 4 that the adsorption data very well embodied Freundlich adsorption isotherm. Freundlich adsorption isotherm fitting has higher correlation coefficients 0.99866, 0.99673, 0.99945, which are greater than 0.99. Freundlich index n is in the range of 1–10, indicated a good adsorption. At the same time, the high adsorption ability indicates that the binding site between the dye molecules and the adsorbent is a strong electrostatic attraction.

3.5. Adsorption thermodynamics

The Gibbs free energy ($\Delta G°$) in the reaction process, the enthalpy change ($\Delta H°$), entropy change ($\Delta S°$) is obtained by the following equations [40,49–51]:

$$K_d = \frac{q_e}{C_e} \tag{7}$$

$$\ln K_d = -\frac{\Delta H°}{RT} + \frac{\Delta S°}{R} \tag{8}$$

$$\Delta G° = \Delta H° - T\Delta S° \tag{9}$$

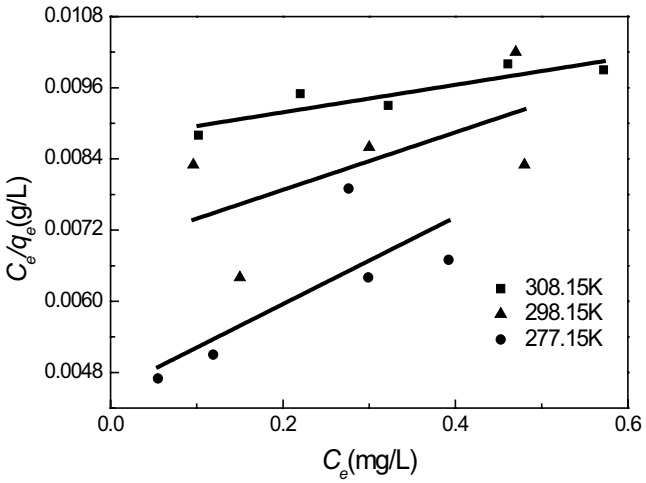

Fig. 2. Langmuir adsorption isotherm.

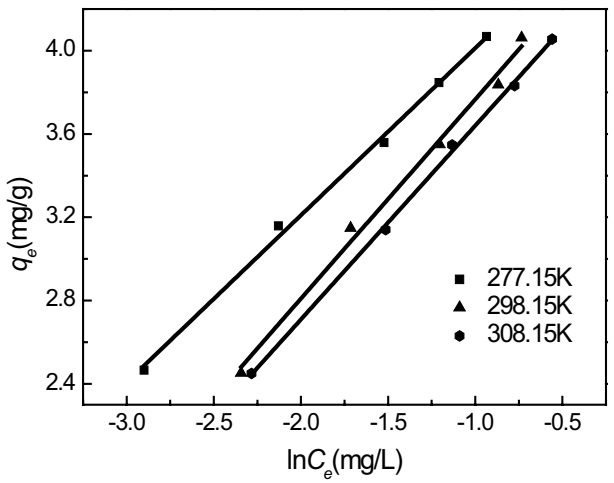

Fig. 3. Freundlich adsorption isotherm.

Table 4
Related parameters of adsorption isotherm

	Langmuir adsorption isotherm			Freundlich adsorption isotherm		
T (K)	q_m (mg g^{-1})	K_L (L mg^{-1})	R^2	K_F (L g^{-1})	$1/n$	R^2
277.15	136.99	1.66	0.48754	123.35	0.80264	0.99866
298.15	206.19	0.70	0.20605	112.52	0.95686	0.99673
308.15	431.03	0.27	0.72904	96.64	0.93067	0.99945

In the above-mentioned equations, R is the ideal gas constant (8.314 J mol^{-1} K^{-1}); T (K) is the absolute temperature; K_d is the adsorption equilibrium constant related to temperature (q_e/C_e).

The thermodynamic parameters of the adsorption of methylene blue by SBA-15 are shown as Table 5, providing Gibbs free energy change (ΔG°), enthalpy change (ΔH°) and entropy change (ΔS°) information. It can be seen from Table 5 that the Gibbs free energy change ΔG° < 0 of the adsorption process, can judge that the adsorption process is spontaneous. ΔG° is from 0 to –20 kJ mol^{-1} which is physical adsorption. –20 to –80 kJ mol^{-1} is physical and chemical adsorption, –80 to –400 kJ mol^{-1} is chemical adsorption. Thus, the adsorption of methylene blue by SBA-15 is a physical adsorption. In the process of adsorption, the enthalpy change, which is –16.623 kJ mol^{-1}, namely ΔH° < 0, shows that the adsorption process is an exothermic reaction. The negative value of entropy indicates that the adsorption process is a process of entropy reduction.

3.6. Characterization of composite materials

Figs. 4 and 5 are low-temperature N_2 adsorption–desorption isotherm of samples and the derived pore size distribution picture: (a) SBA-15 mesoporous material and (b) (SBA-15)-methylene blue composite material. The two samples show hysteresis loop of H1-type, which indicates that the channels are the shape of cylindrical pore. From Fig. 4 it can be seen that the relative partial pressure range after the adsorption of methylene blue is smaller than that before adsorption, this is because the methylene blue molecules were adsorbed into the SBA-15 and occupied the channels of SBA-15, resulting in SBA-15 pore volume decreases. Table 6 is the comparison of the related parameters before and after adsorption of methylene blue dye by SBA-15. Comparing the adsorption properties of two samples before and after the adsorption of methylene blue, it is found that the average pore diameter and pore volume of SBA-15 from 8.33 nm and 1.05 cm^3 g^{-1} were decreased to 6.93 nm and 0.87 cm^3 g^{-1} of (SBA-15)-methylene blue. BET surface area was decreased from 575 to 392 m^2 g^{-1} of (SBA-15)-methylene blue. It can be seen from Fig. 5 that the most probable pore size of after-adsorption is smaller than that of the most probable one before adsorption. It can be seen that after the adsorption of methylene blue, the average pore size, the total pore volume and specific surface area of SBA-15 in the composite material decreased, indicating that after the adsorption of methylene blue the SBA-15 holes were partially filled. This shows that methylene blue molecules were included in the SBA-15 channels, jammed. In Table 1, the molecular diameter of methylene blue given is 0.8 nm. Contrasting the average pore diameter before and after adsorption, it can be calculated that on an average each pore adsorbed 6.67 × 10^{20} methylene blue molecules.

Table 5
Adsorption thermodynamic parameters

T (K)	ΔG° (kJ mol^{-1})	ΔH° (kJ mol^{-1})	ΔS°(J mol^{-1} K^{-1})
277.15	–12.259	–16.623	–15.747
298.15	–11.928		
308.15	–11.771		
318.15	–11.613		

In order to quantitatively calculate the blocking effect of methylene blue on the SBA-15 molecular sieve, the normalized surface area (NSA) of the material was calculated. The NSA value of the composite material [52] can be used to judge the existence state of the object material in the composite:

- When the composite material NSA << 1: the object material will form relatively large particles, these particles

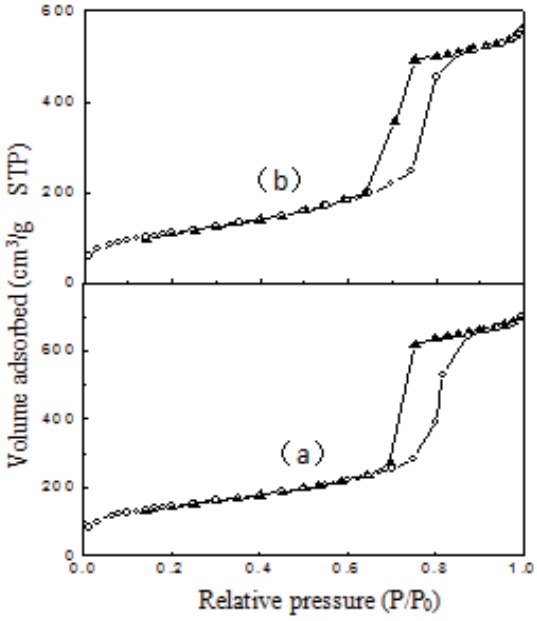

Fig. 4. Low-temperature N_2 adsorption–desorption isotherms of samples (○ adsorption; ▲ desorption). (a) Mesoporous material SBA-15 and (b) (SBA-15)-methylene blue composite material.

go into the molecular sieve, blocking the channels, so that the molecular sieve material pore volume, surface area and pore size decreases rapidly (Fig. 6a).

- When the NSA~1 of the composite material: the object material will form an amorphous layer, closely cover on the inner surface of the molecular sieve (Fig. 6b). As after these particles attach on the inner surface of the molecular sieve, a new surface is formed, only the original surface is covered. Therefore, NSA value of this kind of material is close to 1.
- When the composite material NSA > 1: object material will form very small nanocrystals dispersing in the inner and outer surfaces of molecular sieve (Fig. 6c). As these nano crystal grain sizes are very small, the specific surface area of the composite is greatly increased. Therefore, its NSA value is much more greater than 1.

The NSA is defined as [52]:

$$\mathrm{NSA} = \frac{\mathrm{SA}_1}{1-y} \times \frac{1}{\mathrm{SA}_2} \tag{10}$$

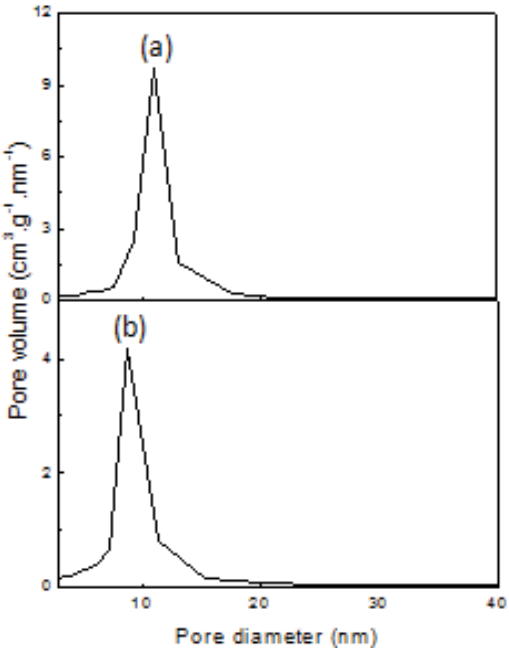

Fig. 5. Pore size distribution of sample. (a) Mesoporous material SBA-15 and (b) (SBA-15)-methylene blue composite material.

where SA_1 and SA_2 are surface area of the (SBA-15)-methylene blue composite and SBA-15, respectively, y is weight fraction of the methylene blue in the composite sample.

In the present study, the NSA value is 0.83 for the (SBA-15)-methylene blue sample. Its NSA is ~1. The methylene blue formed an amorphous layer, closely covered on the inner surface of the molecular sieve (Fig. 6b). As after these particles are attached on the inner surface of the SBA-15 molecular sieve, a new surface was formed and only the original surface was covered.

Fig. 7 shows the X-ray diffraction pattern of mesoporous material SBA-15 and (SBA-15)-methylene blue composite before and after adsorption. It can be seen from the chart that the (SBA-15)-methylene blue composite after the adsorption of methylene blue still retained the characteristic diffraction peaks of mesoporous material SBA-15, indicating that the composite after the adsorption still retained the skeleton structure of mesoporous material SBA-15. From the scanning electron microscopic patterns before and after adsorption as shown in Fig. S9, it can be seen that the two samples are of rod structure, the order after the adsorption is lower than that before the adsorption.

Fig. S10 shows the infrared spectra of the SBA-15 and (SBA-15)-methylene blue from wavenumber 4,000 cm^{-1} to wavenumber 400 cm^{-1}. The 470 cm^{-1} of (SBA-15)-methylene blue and 466 cm^{-1} of SBA-15 are assigned to T–O bend, the 1,054 cm^{-1} of (SBA-15)-methylene blue and 1,092 cm^{-1} of SBA-15 is assigned to the asymmetric stretching vibration. Compared with (a), (b), (c) curves of Fig. S10, the (SBA-15)-methylene blue composite material still has the main characteristic peaks of SBA-15, and the characteristic peaks of

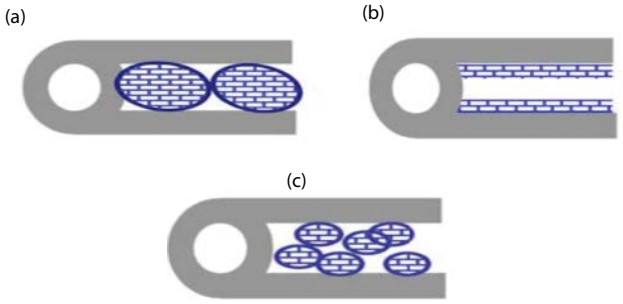

Fig. 6. (a) Main type I of guest phase assembling inside the SBA-15 mesopores, (b) main type II of guest phase assembling inside the SBA-15 mesopores, and (c) main type III of guest phase assembling inside the SBA-15 mesopores.

Table 6
Pore structure parameters of samples

Sample	Crystal plane spacing, d_{100}(nm)	Cell parameter, a_0 (nm)	Thickness of pore wall (nm)	BET surface area ($m^2\ g^{-1}$)	Mesopore volume $cm^3\ g^{-1}$	Average pore diameter, D_p (nm)
SBA-15	9.39	10.84	3.71	575	1.05	8.33
Composite material	10.76	12.42	5.49	392	0.87	6.93

Note: Cell parameter $a_0 = 2 \times d_{100} / \sqrt{3}$.
Average pore diameter $D_p = 4V_{mes}/S_{BET}$. Here V_{mes} is mesoporous volume, S_{BET} is the surface area of BET. Thickness of pore wall = $a_0 - D_p$.

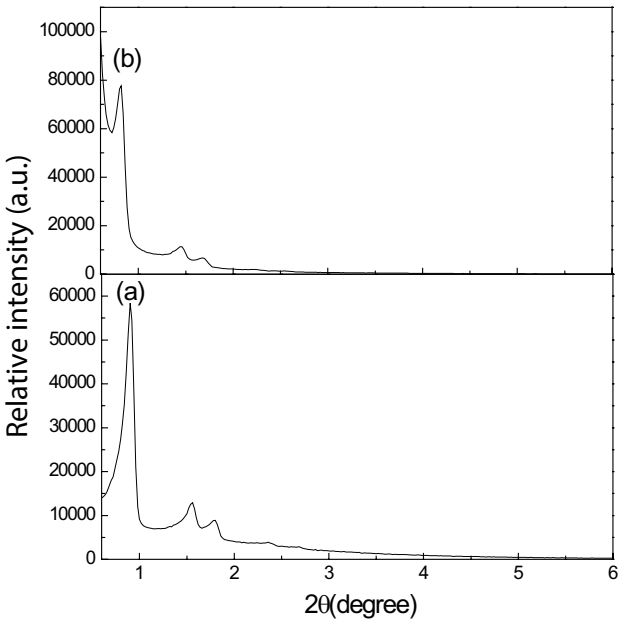

Fig. 7. XRD pattern (a) SBA-15 and (b) (SBA-15)-methylene blue.

methylene blue appear in the wavenumber 669, 1,338 and 1,558 cm^{-1}. 669 cm^{-1} is assigned to the plane outside bending vibration of hydrocarbon on the benzene ring; 1,338 cm^{-1} is assigned to the symmetric deformation vibration of methyl; 1,558 cm^{-1} is assigned to the vibration peak of benzene ring skeleton. It can be explained that (SBA-15)-methylene blue composite material had SBA-15 skeleton structure and contained methylene blue. The reaction mechanism is shown in Fig. 8. Under the alkaline condition, the surface –OH of SBA-15 lost H^+ and the SBA-15 carried a large amount of negative charge. And the methylene blue is a basic cationic dye, in aqueous solution after ionization the colored ions are cations, SBA-15 with a large number of negative charges combined with the colored cations ionized by methylene blue ionization, so as to achieve the effect of adsorption.

4. Conclusion

In this paper, SBA-15 molecular sieve was successfully prepared by hydrothermal method, and through a series of methods powder XRD, SEM, TEM , FT-IR spectra, low-temperature N_2 adsorption–desorption, the SBA-15 and its composite were characterized. The molecular sieve was used as the host for the adsorption of methylene blue dye. The optimal adsorption conditions were obtained: room temperature (20°C ± 1°C), pH = 9, (SBA-15): methylene blue = 8.33, the contact time 40 min, the maximum adsorption capacity and the maximum adsorption removal efficiency of this adsorption system for methylene blue are 223 mg g^{-1} and 97.5%, respectively. At the same time, the kinetic and thermodynamic calculations were carried out, and the kinetic data showed that the adsorption process is in accordance with the quasi-second-order kinetic equation. The analysis of adsorption isotherms showed that the Freundlich adsorption curve was more suitable for the adsorption of methylene blue on SBA-15. Thermodynamic corresponding calculation obtained the thermodynamic properties parameters $\Delta H° < 0$, $\Delta S° < 0$, $\Delta G° < 0$, proving that the process of adsorption of methylene blue by SBA-15 is the physical adsorption process of entropy reduction. The characterization of the composite could prove that the methylene blue is adsorbed into the SBA-15 channels. The adsorption process was completed by physical adsorption and chemical adsorption of methylene blue with SBA-15. The result is the synergistic action of the electrostatic force, hydrogen bond and so on.

Acknowledgments

The authors would like to thank the reviewers and editor who gave many excellent comments and suggestions on this article.

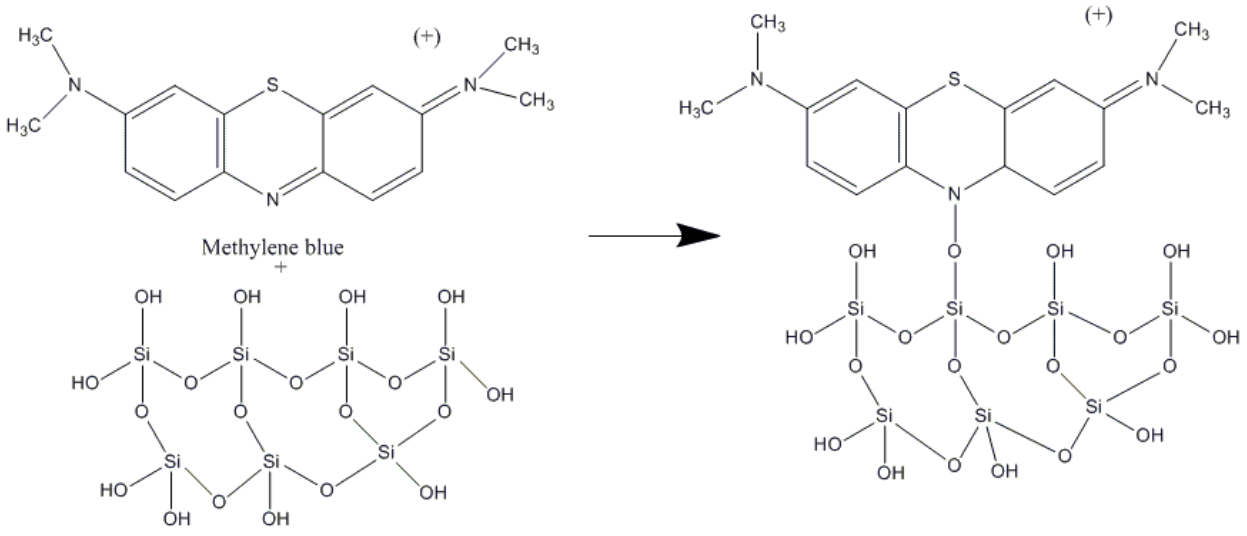

Fig. 8. Diagram of reaction mechanism.

References

[1] C. Fleischmann, M. Lievenbruck, H. Ritter, Polymers and dyes: developments and applications, Polymers, 7 (2015) 717–746.

[2] P.T. Chou, Y. Chi, Phosphorescent dyes for organic light-emitting diodes, Chemistry, 13 (2007) 380–395.

[3] Y. Tatsumi, M. Inoue, Development of color resists containing novel dyes for liquid crystal displays, Sumitomo Chem., 5 (2016) 521–523.

[4] K. Peneva, Design, Synthesis and Application of Ultrastable Rylene Dyes for Fluorescent Labeling of Biomolecules, Ph.D. Thesis, Johannes Gutenberg-Universität, Mainz, 7 (2016) 1–9.

[5] B.H. Hameed, A.A. Ahmad, Batch adsorption of methylene blue from aqueous solution by garlic peel, an agricultural waste biomass, J. Hazard. Mater., 164 (2009) 870–875.

[6] B. Yasemin, A. Haluk, A kinetics and thermodynamics study of methylene blue adsorption on wheat shells, Desalination, 194 (2006) 259–267.

[7] M.R. Sohrabi, M. Ghavami, Photocatalytic degradation of Direct Red 23 dye using UV/TiO_2: effect of operational parameters, J. Hazard. Mater., 153 (2008) 1235–1239.

[8] M. Sleiman, D. Vildozo, C. Ferronato, J.-M. Chovelon, Photocatalytic degradation of azo dye Metanil Yellow: optimization and kinetic modeling using a chemometric approach, Appl. Catal., B, 77 (2007) 1–11.

[9] M. Abbasi, N.R. Asl, Sonochemical degradation of basic blue 41 dye assisted by nano TiO_2 and H_2O_2, J. Hazard. Mater., 153 (2008) 942–947.

[10] N. Zaghbani, A. Hafiane, M. Dhahbi, Removal of Safranin T from wastewater using micellar enhanced ultrafiltration, Desalination, 222 (2008) 348–356.

[11] J.-S. Wu, C.-H. Liu, K.H. Chu, S.-Y. Suen, Removal of cationic dye methyl violet 2B from water by cation exchange membranes, J. Membr. Sci., 309 (2008) 239–245.

[12] L. Fan, Y. Zhou, W. Yang, G. Chen, F. Yang, Electrochemical degradation of aqueous solution of Amaranth azo dye on ACF under potentiostatic model, Dyes Pigm., 76 (2008) 440–446.

[13] M.-X. Zhu, L. Lee, H.-H. Wang, Z. Wang, Removal of an anionic dye by adsorption/precipitation processes using alkaline white mud, J. Hazard. Mater., 149 (2007) 735–741.

[14] Mohd. Rafatullah, O. Sulaiman, R. Hashim, A. Ahmad, Adsorption of methylene blue on low-cost adsorbents: a review, J. Hazard. Mater., 177 (2010) 70–80.

[15] Y. Feng, H. Zhou, G. Liu, J. Qiao, J. Wang, H. Lu, L. Yang, Y. Wu, Methylene blue adsorption onto swede rape straw (*Brassica napus* L.) modified by tartaric acid: equilibrium, kinetic and adsorption mechanisms, Bioresour. Technol., 125 (2012) 138–144.

[16] K. Porkodi, K.V. Kumar, Equilibrium, Kinetics and mechanism modeling and simulation of basic and acid dyes sorption onto jute fiber carbon: eosin yellow, malachite green and crystal violet single component systems, J. Hazard. Mater., 143 (2007) 311–327.

[17] V. Katheresan, J. Kansedo, S.Y. Lau, Efficiency of various recent wastewater dye removal methods: a review, J. Environ. Chem. Eng., 6 (2018) 4676–4697.

[18] H. Javadian, M.T. Angaji, M. Naushad, Synthesis and characterization of polyaniline/γ-alumina nanocomposite: a comparative study for the adsorption of three different anionic dyes, J. Ind. Eng. Chem., 20 (2014) 3890–3900.

[19] G. Sharma, Mu. Naushad, A. Kumar, S. Rana, S. Sharma, A. Bhatnagar, F.J. Stadler, A.A. Ghfar, M.R. Khan, Efficient removal of coomassie brilliant blue R-250 dye using starch/poly(alginic acid-*cl*-acrylamide) nanohydrogel, Process Saf. Environ. Prot., 109 (2017) 301–310.

[20] H. Chaudhuri, S. Dash, A. Sarkar, SBA-15 functionalised with high loading of amino or carboxylate groups as selective adsorbent for enhanced removal of toxic dyes from aqueous solution, New J. Chem., 40 (2016) 3622–3634.

[21] H. Chaudhuri, S. Dash, A. Sarkar, Fabrication of new synthetic routes for functionalized Si-MCM-41 materials as effective adsorbents for water remediation, Ind. Eng. Chem. Res., 55 (2016) 10084–10094.

[22] O.S. Amuda, A.O. Olayiwola, A.O. Alade, A.G. Farombi, S.A. Adebisi, Adsorption of methylene blue from aqueous solution using steam-activated carbon produced from *Lantana camara* stem, J. Environ. Prot., 5 (2014) 1352–1363.

[23] E.I. El-Shafey, S.N.F. Ali, S. Al-Busafi, H.A.J. Al-Lawati, Preparation and characterization of surface functionalized activated carbons from date palm leaflets and application for methylene blue removal, J. Environ. Chem. Eng., 4 (2016) 2713–2724.

[24] A.B. Albadarin, M.N. Collins, Mu. Naushad, S. Shirazian, G. Walker, C. Mangwandi, Activated lignin-chitosan extruded blends for efficient adsorption of methylene blue, Chem. Eng. J., 307 (2017) 264–272.

[25] M. Ghaedi, M.D. Ghazanfarkhani, S. Khodadoust, N. Sohrabi, M. Oftade, Acceleration of methylene blue adsorption onto activated carbon prepared from dross licorice by ultrasonic method: equilibrium, kinetic and thermodynamic studies, J. Ind. Eng. Chem., 20 (2014) 2548–2560.

[26] O.A. Attallah, M.A. Al-Ghobashy, M. Nebsen, M.Y. Salem, Removal of cationic and anionic dyes from aqueous solution with magnetite/pectin and magnetite/silica/pectin hybrid nanocomposites: kinetic, isotherm and mechanism analysis, RSC Adv., 6 (2016) 11461–11480.

[27] F. Ge, H. Ye, M.-M. Li, B.-X. Zhao, Efficient removal of cationic dyes from aqueous solution by polymer-modified magnetic nanoparticles, Chem. Eng. J., 198 (2012) 11–17.

[28] K.T. Wong, N.C. Eu, S. Ibrahim, H. Kim, Y. Yoon., M. Jang, Recyclable magnetite-loaded palm shell-waste based activated carbon for the effective removal of methylene blue from aqueous solution, J. Cleaner Prod., 115 (2016) 337–342.

[29] E. Haque, V. Lo, A.I. Minett, A.T. Harris, T.L. Church, Dichotomous adsorption behaviour of dyes on an amino-functionalised metal–organic framework, amino-MIL-101(Al), J. Mater. Chem. A, 2 (2014) 193–203.

[30] C. Li, Z. Xiong, J. Zhang, C. Wu, The strengthening role of the amino group in metal–organic framework MIL-53 (Al) for methylene blue and malachite green dye adsorption, J. Chem. Eng. Data, 60 (2015) 3414–3422.

[31] A.A. Alqadami, M. Naushad, Z.A. Alothman, T. Ahamad, Adsorptive performance of MOF nanocomposite for methylene blue and malachite green dyes: kinetics, isotherm and mechanism, J. Environ. Manage., 223 (2018) 29–36.

[32] D. Zhao, J. Feng, Q. Huo, N. Melosh, G.H. Fredrickson, B.F. Chmelka, G.D. Stucky, Triblock copolymer syntheses of mesoporous silica with periodic 50 to 300 angstrom pores, Science, 279 (1998) 548–552.

[33] A. Salis, D. Meloni, S. Ligas, M.F. Casula, M. Monduzzi, V. Solinas, E. Dumitriu, Physical and chemical adsorption of *Mucor javanicus* lipase on SBA-15 mesoporous silica. Synthesis, structural characterization, and activity performance, Langmuir, 21 (2005) 5511–5516.

[34] X. Xu, H. Mu, A.R.H. Skands, C.E. Hou, J. Adler-Nissen, Parameters affecting diacylglycerol formation during the production of specific-structured lipids by lipase-catalyzed interesterification, J. Am. Oil Chem. Soc., 76 (1999) 175–181.

[35] J.C.P. Broekhoff, J.H.D. Boer, Studies on pore systems in catalysts: XII. Pore distributions from the desorption branch of a nitrogen sorption isotherm in the case of cylindrical pores A. An analysis of the capillary evaporation process, J. Catal., 10 (1968) 391–400.

[36] S. Brunauer, P.H. Emmett, E. Teller, Adsorption of gases in multimolecular layers, J. Am. Chem. Soc., 60 (1938) 309–319.

[37] E.P. Barrett, L.G. Joyner, P.P. Halenda, The determination of pore volume and area distributions in porous substances. I. Computations from nitrogen isotherms, J. Am. Chem. Soc., 73 (1951) 373–380.

[38] S. Lagergren, Zur theorie der sogenannten adsorption geloester stoffe (About the theory of so-called adsorption of soluble substances), K. Sven. Vetenskapsakad. Handl., 24 (1898) 1–39.

[39] G. Crini, H.N. Peindy, F. Gimbert, C. Robert. Removal of C.I. basic green 4 (malachite green) from aqueous solutions by adsorption using cyclodextrin-based adsorbent: kinetic and equilibrium studies, Sep. Purif. Technol., 53 (2007) 97–110.

[40] M. Naushad, Surfactant assisted nano-composite cation exchanger: development, characterization and applications for the removal of toxic Pb^{2+} from aqueous medium, Chem. Eng. J., 235 (2014) 100–108.
[41] Y.S. Ho, G. McKay, Pseudo-second order model for sorption processes, Process Biochem., 34 (1999) 451–465.
[42] I. Langmuir, The constitution and fundamental properties of solids and liquids, J. Am. Chem. Soc., 38 (1916) 2221–2295.
[43] I. Langmuir, The adsorption of gases on plane surfaces of glass mica platinum, J. Am. Chem. Soc., 40 (1918) 1361–1403.
[44] A.A. Alqadami, Mu. Naushad, Z.A. Alothman, A.A. Ghfar, Novel metal–organic framework (MOF) based composite material for the sequestration of U(VI) and Th(IV) metal ions from aqueous environment, ACS Appl. Mater. Interfaces, 9 (2017) 36026–36037.
[45] H. Freundlich, Uber die adsorption in losungen (Over the adsorption in solution), Zeitschift fur Physikalische Chemie (J. Phys. Chem.), 57 (1906) 385–470.
[46] Z.A. Al-Othman, R. Ali, Mu. Naushad, Hexavalent chromium removal from aqueous medium by activated carbon prepared from peanut shell: adsorption kinetics, equilibrium and thermodynamic studies, Chem. Eng. J., 184 (2012) 238–247.
[47] Mu. Naushad, T. Ahamad, B.M. Al-Maswari, A.A. Alqadami, S.M. Alshehri, Nickel ferrite bearing nitrogen-doped mesoporous carbon as efficient adsorbent for the removal of highly toxic metal ion from aqueous medium, Chem. Eng. J., 330 (2017) 1351–1360.
[48] Y. Shu, Y. Shao, X. Wei, X. Wang, Q. Sun, Q. Zhang, L. Li, Synthesis and characterization of Ni-MCM-41 for methyl blue adsorption, Microporous Mesoporous Mater., 214 (2015) 88–94.
[49] S. Chowdhury, R. Mishra, P. Saha, P. Kushwaha, Adsorption thermodynamics, kinetics and isosteric heat of adsorption of malachite green onto chemically modified rice husk, Desalination, 265 (2011) 159–168.
[50] Y. Zhou, M. Zhang, X. Hu, X. Wang, J. Niu, T. Ma. Adsorption of cationic dyes on a cellulose-based multicarboxyl adsorbent, J. Chem. Eng. Data, 58 (2013) 413–421.
[51] Mu. Naushad, T. Ahamad, G. Sharma, A.H. Al-Muhtaseb, A.B. Albadarin, M.M. Alam, Z.A. Alothman, S.M. Alshehri, A.A. Ghfar, Synthesis and characterization of a new starch/SnO_2 nanocomposite for efficient adsorption of toxic Hg^{2+} metal ion, Chem. Eng. J., 300 (2016) 306–316.
[52] L. Vradman, M.V. Landau, D. Kantorovich, Y. Koltypin, A. Gedanken, Evaluation of metal oxide phase assembling mode inside the nanotubular pores of mesostructured silica, Microporous Mesoporous Mater., 79 (2005) 307–318.

Supplementary Information

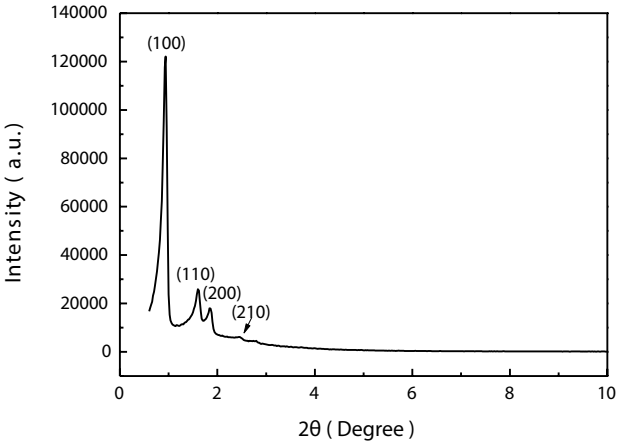

Fig. S1. XRD pattern of mesoporous material SBA-15.

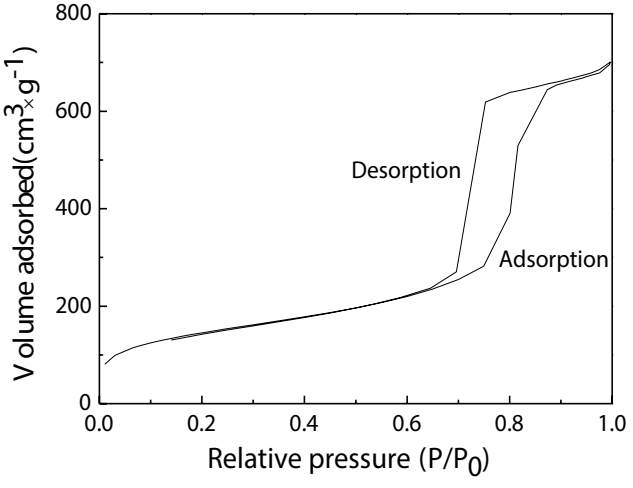

Fig. S2. Low-temperature nitrogen adsorption–desorption curve of SBA-15.

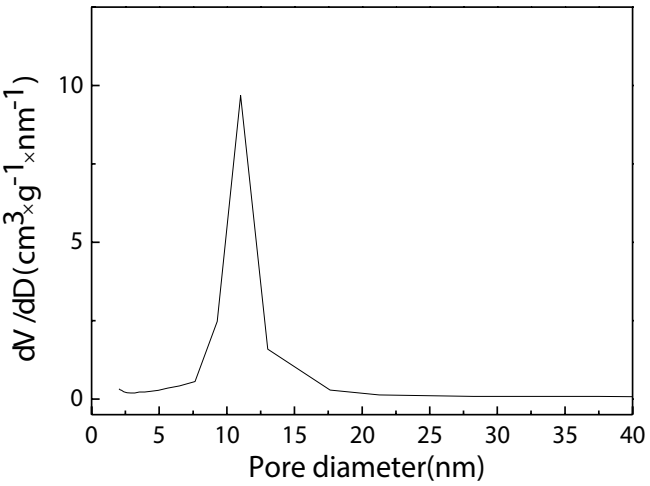

Fig. S3. Pore size distribution of SBA-15.

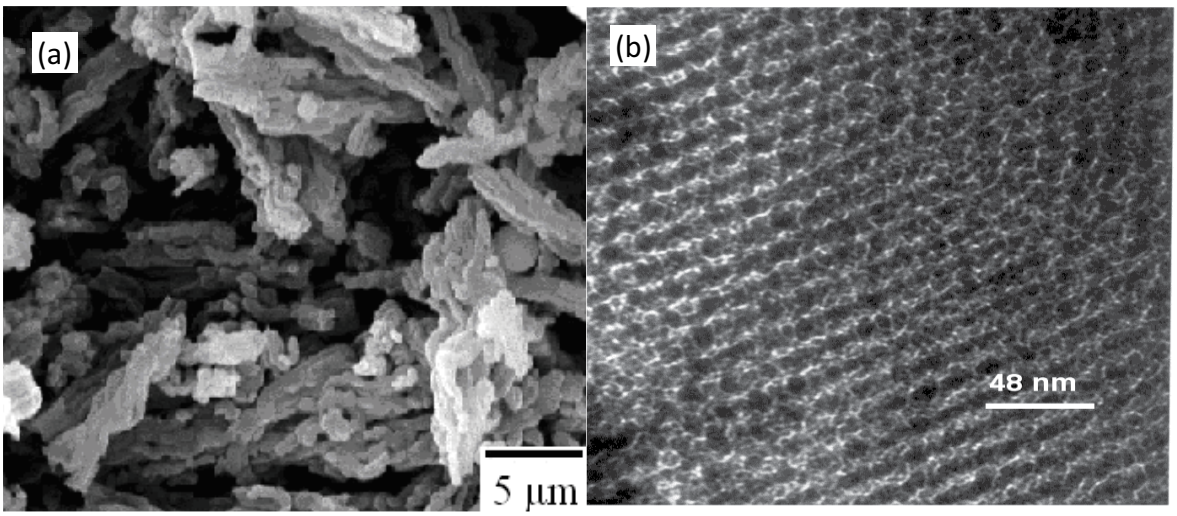

Fig. S4. (a) Scanning electron microscopic and (b) transmission electron microscopic images of SBA-15.

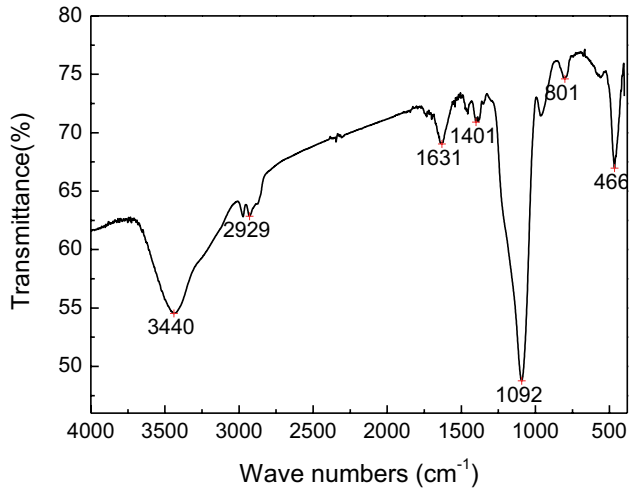

Fig. S5. Infrared spectrum of SBA-15.

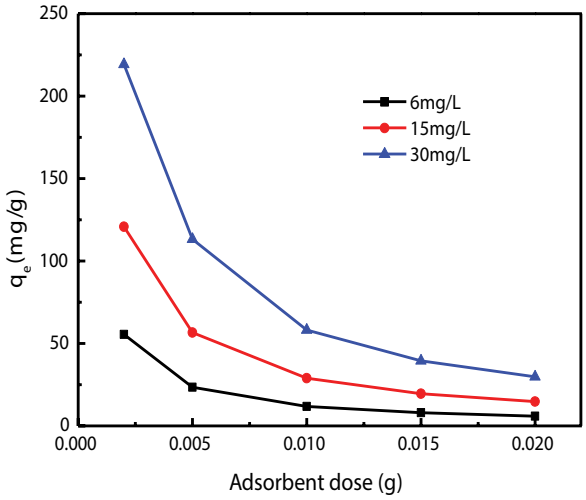

Fig. S7. Effect of adsorbent dosage on the adsorption of dye.

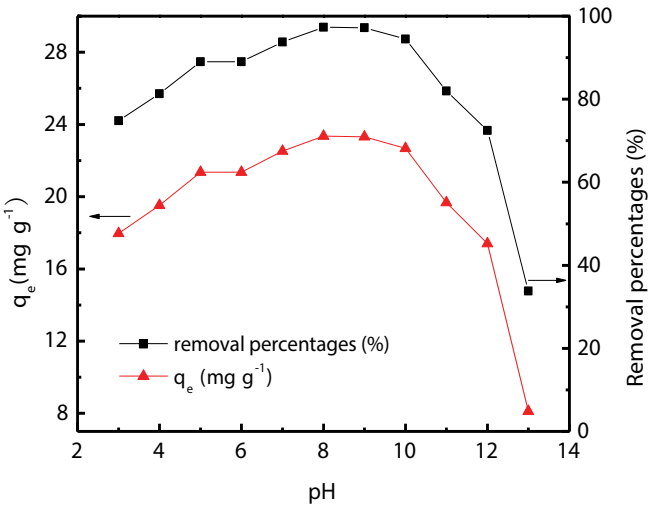

Fig. S6. Effect of pH on the adsorption amount of dye.

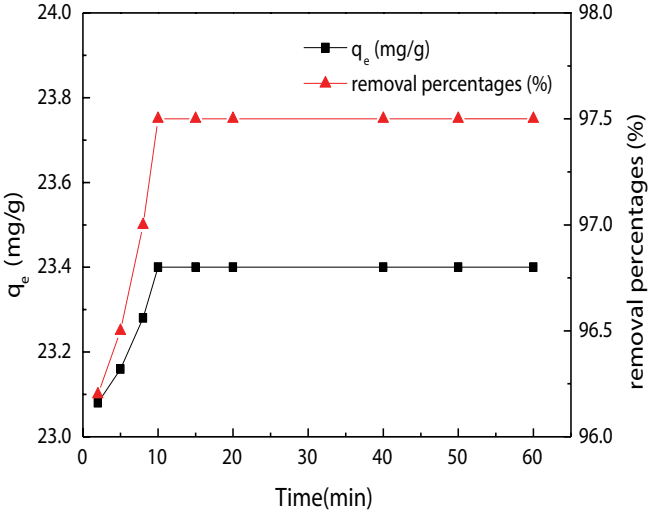

Fig. S8. Effect of contact time on the adsorption of dye.

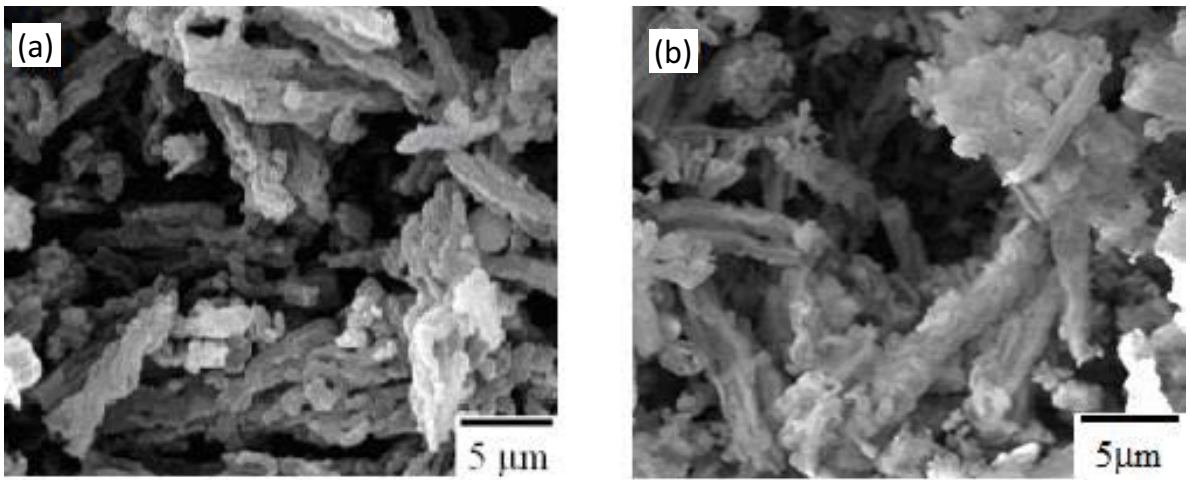

Fig. S9. Scanning electron microscopic images of samples: (a) SBA-15 and (b) (SBA-15)-methylene blue.

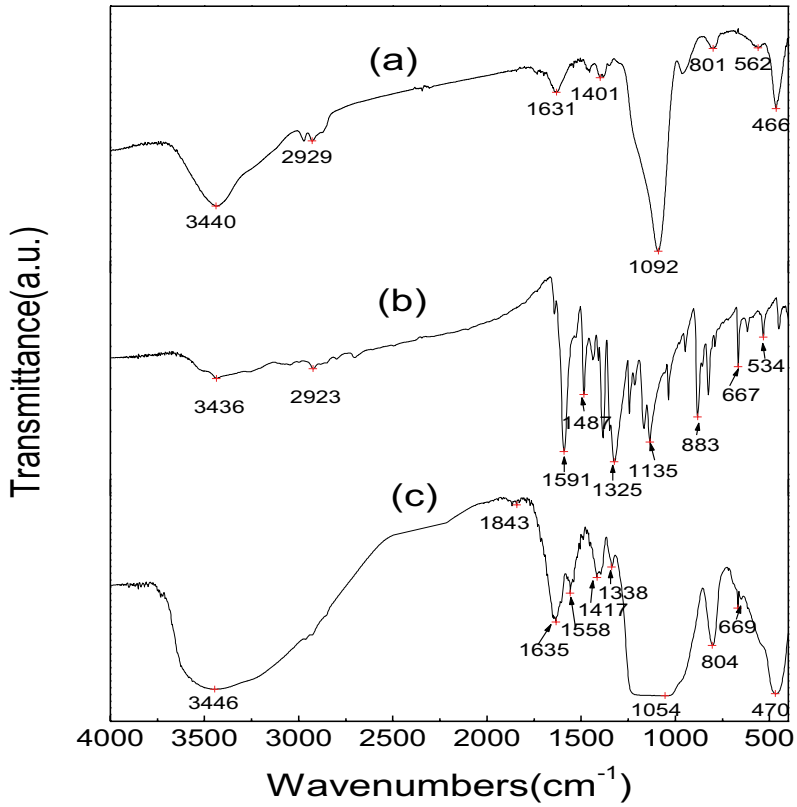

Fig. S10. Infrared spectra: (curve a) SBA-15, (curve b) methylene blue, and (curve c) (SBA-15)-methylene blue.

Table S1
Structural parameters of SBA-15

X-ray diffraction			Nitrogen adsorption at low temperature		
Interplanar spacing, d_{100} (nm)	Lattice parameter, a_0 (nm)	Pore wall thickness (nm)	BET surface area ($m^2\ g^{-1}$)	Mesopore volume ($cm^3\ g^{-1}$)	Average pore diameter of D_p (nm)
9.39	10.84	2.51	575	1.05	8.33

Note: Cell parameters $a_0 = 2 \times d_{100} / \sqrt{3}$.
Average pore diameter $D_p = 4V_{mes}/S_{BET}$. Here V_{mes} is mesoporous volume, S_{BET} is the surface area of BET. Thickness of pore wall = $a_0 - D_p$.